2012

Screen-printing of ferrite magnetic nanoparticles produced by carbon combustion synthesis of oxides

Karen S. Martirosyan
The University of Texas Rio Grande Valley

Gamage Dannangoda
The University of Texas Rio Grande Valley

Eduard Galstyan
University of Houston

Dmitri Litvinov
University of Houston

Recommended Citation

Martirosyan, Karen S., et al. "Screen-Printing of Ferrite Magnetic Nanoparticles Produced by Carbon Combustion Synthesis of Oxides." Journal of Applied Physics, vol. 111, no. 9, American Institute of Physics, May 2012, p. 094311, doi:10.1063/1.4711097.

Screen-printing of ferrite magnetic nanoparticles produced by carbon combustion synthesis of oxides

Karen S. Martirosyan,[1,a)] Chamath Dannangoda,[1] Eduard Galstyan,[2] and Dmitri Litvinov[3]
[1]*Department of Physics and Astronomy, University of Texas at Brownsville, Brownsville, Texas 78520, USA*
[2]*Texas Center for Superconductivity, University of Houston, Houston, Texas 77204, USA*
[3]*Department of Electrical and Computer Engineering, University of Houston, Houston, Texas 77204, USA*

(Received 26 February 2012; accepted 14 April 2012; published online 7 May 2012)

The feasibility of screen-printing process of hard ferrite magnetic nanoparticles produced by carbon combustion synthesis of oxides (CCSO) is investigated. In CCSO, the exothermic oxidation of carbon generates a smolder thermal reaction wave that propagates through the solid reactant mixture converting it to the desired oxides. The complete conversion of hexaferrites occurs using reactant mixtures containing 11 wt. % of carbon. The $BaFe_{12}O_{19}$ and $SrFe_{12}O_{19}$ hexaferrites had hard magnetic properties with coercivity of 3 and 4.5 kOe, respectively. It was shown that the synthesized nanoparticles could be used to fabricate permanent magnet structures by consolidating them using screen-printing techniques. © *2012 American Institute of Physics*.
[http://dx.doi.org/10.1063/1.4711097]

INTRODUCTION

A hard magnetic hexaferrite with basic formula $MeFe_{12}O_{19}$, (where Me-Ba or Sr), has been widely used as a permanent magnets due to their very low electrical conductivity, high magnetic anisotropy, high Curie temperature, mechanical hardness, excellent chemical stability, and corrosion resistivity.[1,2] Recent studies have focused on the synthesis of nanocrystalline powders in order to improve magnetic properties with increasing the surface area of the nanopowders to enable use in elastic magnetic materials. There has recently been increasing interest also in the use of $MeFe_{12}O_{19}$ hexaferrite in the recording media applications with the emphasis on high-density perpendicular magnetic recording[3,4] where nanocrystalline magnetic thin-film media is required. Furthermore, the nanoscale magnetic ferrites are of particular interest due to their chemical compatibility with biological tissues and their unique combination of electronic and magnetic properties.[5]

$MeFe_{12}O_{19}$ hexaferrite particles can be produced by several processes, which differ in the production price and product properties. The oldest and most common one involves calcinations of a mixture of blended reactants (oxides or carbonates) in a furnace at temperature of up to 1200 °C for periods of 2–8 h.[6,7] This method requires use of high-temperature furnaces and high-energy consumption. Due to the long processing at high temperatures, the resultant particulate size of ferrite powders produced by calcination is large and requires further extensive processing to reduce grain size to enable desired magnetic properties. Several methods such as co-precipitation, glass crystallization, hydrothermal synthesis, sol–gel techniques, organo-metallic, microemulsion, spray deposition, organic ligand-assisted supercritical water process, and other processes have been developed for preparing nanoparticles of barium ferrite.[8,9] However, all wet-chemical methods have several drawbacks: high *p*H sensitivity, stringent drying conditions, use of complex equipment and expensive precursors, and disposal of the by-product. Also, most of the wet-chemical methods produce an amorphous structure that requires, in general, calcination at a high temperature to obtain a product with the desired magnetic properties and crystal structure. While the wet chemical processes can produce high quality powders, the production costs are much higher than in calcination. The cost-effective preparation of mono-disperse particles of ferrites in the nano size (less than 100 nm) remains a challenge.

A novel method to produce ferrite nanoparticles by *carbon combustion synthesis of oxides* (CCSO) is recently proposed.[10–13] $C + O_2 = CO_2\ \Delta H^{298}_{CO_2} = -393.5$ kJ/mol generates a thermal reaction wave with relatively low temperatures at 600–1000 °C that propagate at a velocity of 0.1–4 mm/s through the solid reactant mixture converting it to the desired oxide product by the reaction $\sum_{i=1}^{n} \mu_i X_i^{(s)} + \alpha C^{(s)} + \beta O_2^{(g)} = \sum_{j=1}^{m} P_j^{(s)} + \delta CO_2^{(g)} + (-\Delta H)$, where $\alpha = \frac{x/12}{(100-x)/\sum \mu_i M_i^{(s)}}$ and $X_i^{(s)}$ are the solid compound (such as an oxide, super oxide, nitride, or carbonate, chloride, or oxalate) containing the metal needed to form the oxide; $P_j^{(s)}$ is the solid complex oxide product; μ_I, β, and δ are the stoichiometric coefficients; $(-\Delta H)$ is the heat of the reaction; x is the carbon weight percent in the mixture; $M_i^{(s)}$ is the molecular weight of the ith reactant. This method was successfully applied for simple, economical, and energy efficient production of several complex oxides nanoparticles.[10–13] The motivation of this study was to test a feasibility of screen-printing process of hard ferrite magnetic nanoparticles produced by CCSO. Furthermore, a process for deposition of magnetic nanoparticles by using dispensing robot is described.

EXPERIMENTAL PART

Barium and strontium hexaferrite nanoparticles were produced by CCSO via the following reaction:

a)Electronic mail: karen.martirosyan@utb.edu.

$$MeCO_3 + 6Fe_2O_3 + \alpha(C + O_2) = MeFe_{12}O_{19} + (\alpha+1)CO_2, \quad (1)$$

where Me = Ba or Sr. The high purity (99.9%) reactants mixture used in CCSO contained 11 wt. % carbon nanoparticles "carbon acetylene" with the average particle size of 5 nm (surface area ~ 80 m^2/g) and non-combustible iron oxide and barium or strontium carbonate reactants. The molar ratio among the reactants was set according to the stoichiometry of $BaFe_{12}O_{19}$ and $SrFe_{12}O_{19}$. The reactants were dried at 115 °C for 5 h before mixture preparation. Then, the reactants thoroughly mixed together by using high energy milling for about 2 h. The combustion synthesis was conducted by loading a loose mixture into a ceramic boat that was placed inside a cylindrical stainless steel vessel (ID = 70-mm and 60-mm length) fed by oxygen at a flow rate at 10 l/min. To initiate the propagating temperature front, the reactant mixture was locally ignited by an electrically heated coil.

The composition and crystal structure of the products were analyzed by x-ray diffraction (Siemens D5000 diffractometer) with Cu K_α radiation ($\lambda = 1.54056$ Å). Particle morphological features and microprobe analysis were determined by scanning electron microscopy (SEM; JEOL JAX8600, Japan) of loose powder fixed to a graphite disk. Particle size distribution and the particles surface area were determined by a Coulter SA 3100 BET analyzer.

The layers of strontium and barium ferrites were printed by dispensing stabilized magnetic suspension using a composite solution of 7 wt. % ferrite dispersed into poly(methyl methacrylate) (PMMA) solution in dimethylformamide (DMF). We used PMMA as a thickener agent to keep nanoparticles together on the substrate. A polymer solution was dispensed by using the Automated Dispensing Robot (EFD-325TT Dispenser). Its unique features make this dispensing robot a true 3-dimensional motion control system, offering reliable operation with an excellent repeatability for dispensing different types of fluids. The system offers the following features facilitating dispensing of solutions with nanoparticles: (1) closed-loop servo controls providing fast, accurate positioning; (2) fully integrated positioning and dispensing functions; (3) easy programming with the Palm handheld via Bluetooth; and (4) height sensor for critical deposit control.

RESULTS AND DISCUSSION

The x-ray pattern of as-synthesized powders (Figure 1) showed that combustion produced almost pure strontium and barium hexaferrite and did not require further calcinations to complete the reactants conversion. However, an x-ray pattern of as-synthesized $SrFe_{12}O_{19}$ powder shows a low intensity following suggestion that partial amorphous structure (Figure 1(a)) was presented, while for the $BaFe_{12}O_{19}$ powder (Figure 1(b)) was well crystalline and had a flat background, indicating that no amorphous phase was present. The lattice parameters of the barium and strontium hexaferrites were $a = 5.892$ Å, $c = 23.386$ Å and $a = 5.889$ Å, $c = 23.034$ Å, respectively. These data are in a close agreement with published values in the Joint Committee on Powder Diffraction Standards (JCPDS), International Center for diffraction Data. The carbon content of the as-synthesized product was determined by a carbon analyzer (Leco, WR-112), which indicated that the concentration of the residual carbon was less than 0.1 wt. %. All as-synthesized barium and strontium ferrite powders were friable and had a spongy porous structure with porosity of ~70%. The SEM images of the as-synthesized barium ferrite are shown in Figure 1. The combustion products were predominantly rectangular particles with a range of particle size of 50–100 nm. The specific surface area (S) of a non-porous spherical particle is inversely proportional to its diameter, i.e., $S = 6/\rho.D$, where S-(m^2/g), D is the particle size (m), and ρ is the theoretical density,

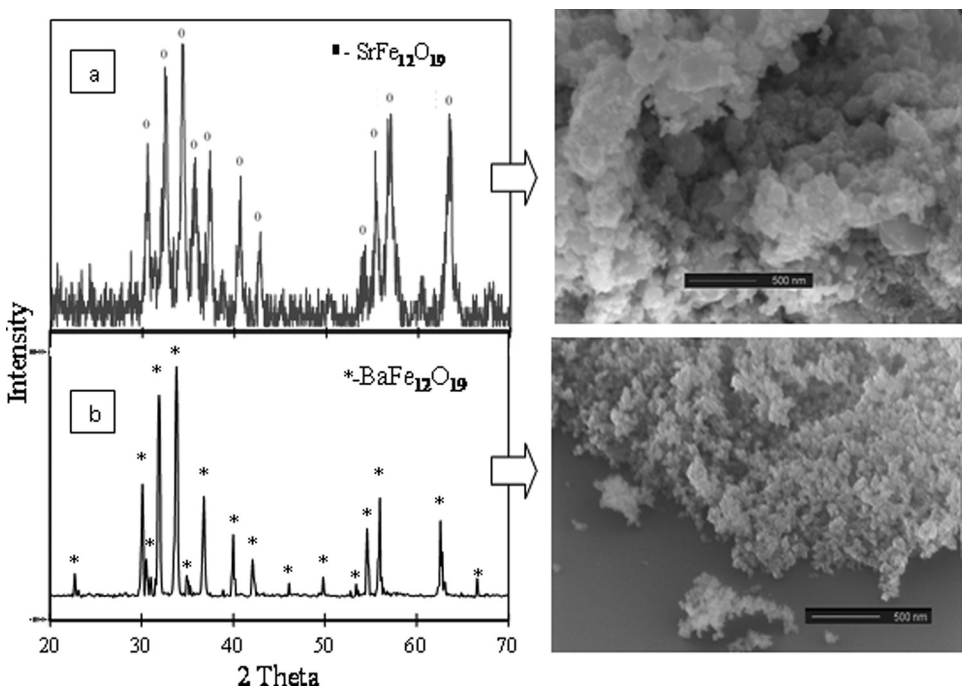

FIG. 1. X-ray diffraction pattern and SEM images of as-synthesized powders at 11 wt. % carbon in the mixture; (a)—$SrFe_{12}O_{19}$ and (b)–$BaFe_{12}O_{19}$.

(g/m^3). From image analysis performed on micrographs the mean diameter of the nanoparticles estimated to be ~60 nm. Assuming that the as-synthesized particles are spherical with density $\rho = 5\ g/cm^3$; then, specific surface area is estimated to be ~20 m^2/g. This data were confirmed by Brunauer-Emmett-Teller (BMT) analysis that shows $S \sim 22\ m^2/g$.

The as-synthesized ferrites powders were washed with alcohol and centrifuged several times to remove any non-react carbon. Thereafter, ethylene glycol (150 ml) and oleic acid (10 ml) were added to the powder (1 g), which was kept at 150 °C for 4 h. Finally, the modified ferrite nanoparticles were dispersed in alcohol solvent with ultrasonic oscillation and centrifuging treatment to remove excess of oleic acid and ethylene glycol. Then, the nanoparticles were dried in a vacuum oven at 50 °C for 4 h. Oleic acid is one of the most widely used surfactants having long chain hydrocarbons. The nanoparticles and PMMA solutions were prepared by mixing surface modified ferrites with 2 wt. % PMMA dissolved in N,N-DMF. After sonication, the ferrofluids were temporarily stable against gravitational as well as magnetic field gradient. Extensive set of experiments shows that the exposition time when ferrite nanoparticles homogeneously dispersed into the PMMA was about 2 h.

The schematic diagram of the EFD dispenser printing system is shown in Figure 2(a). In the print head, the pressure controller changes pressure impulse within the ink chamber, expelling a single tiny droplet from the orifice. The chamber is refilled through the inlet by capillary action at the orifice. The thin film layers are deposited onto the substrate within a predefined printed pattern. AFM image of the micro layer presented in Figure 2(b) shows uniform strontium ferrite particles distributions and confirmed that the average particle size was predominantly ~60 nm. The thickness of the layer was measured by profilometer and estimated to be ~10 μm.

The magnetic properties of the samples were measured at room temperature using a vibrating sample magnetometer vibrating sample magnetometer (VSM) (Lake Shore Cryotronics, Inc., Model 7300) with an applied field up to 10^4 Oe. The magnetic hysteresis loops of screen-printed strontium and barium hexaferrites are presented in Figure 3. The samples show typical hard magnetic properties originated from high magnetocrystalline anisotropy. According to Stoner-Wohlfarth theory,[14] the coercivity field H_c can be determined by relation of magnetocrystalline anisotropy constant K and saturation magnetization M_s: $H_c = 2K/(\mu_\sigma M_s)$, where μ_σ is the universal constant of permeability in free space, $4\pi \times 10^{-7}$ H/m. Thus, from hysteresis loops (Fig. 3), the K can be calculated combining the results of H_c and M_s which are 4.5 kOe and 57 emu/g for $SrFe_{12}O_{19}$ and 3 kOe and 36 emu/g for $BaFe_{12}O_{19}$. So, it can be easily estimated that the value of K for as-prepared $SrFe_{12}O_{19}$ is higher than that for $BaFe_{12}O_{19}$ sample that is in a good agreement with a theoretical work.[15] Since the anisotropy constant, K, is proportional to energy barrier, the rotation of magnetization orientation requires work to be performed against the anisotropy forces and higher fields are required to reverse the spins. It is worth to note that obtained M_s and H_c are smaller than theoretically predicted values for the single crystals;[15]

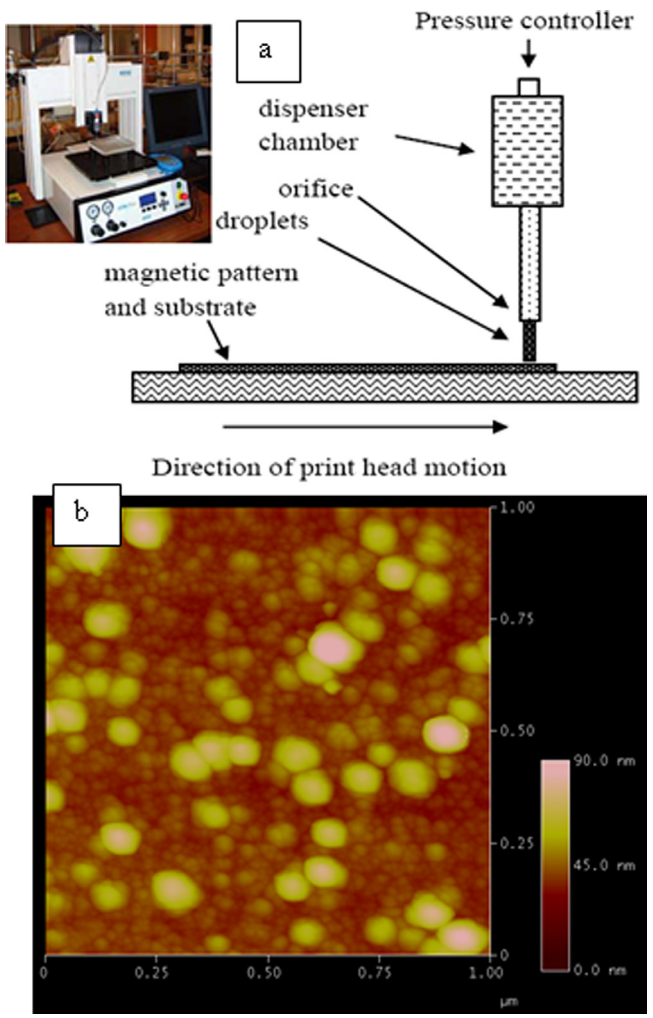

FIG. 2. Screen-printing system and AFM image of thin layer of magnetic $SrFe_{12}O_{19}$ composites.

however, these values comparable to some reported ferrite powders prepared by different chemical methods.[16–19] The absence of fully magnetization saturation is apparently related to a randomly orientation of crystallographic c-axis, the

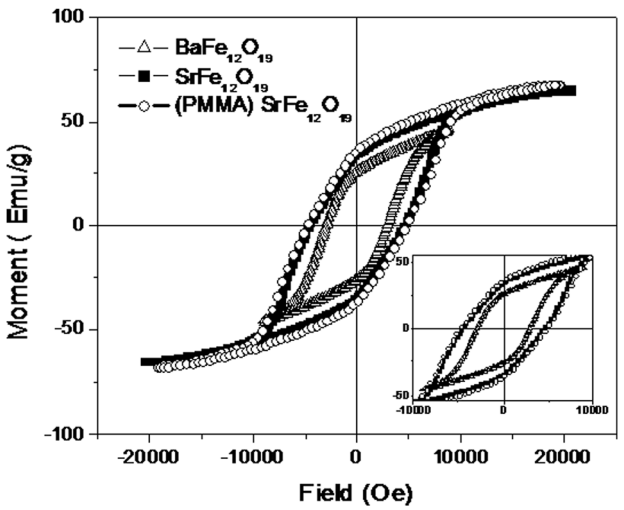

FIG. 3. Magnetic hysteresis loop of screen-printed strontium (round symbol), barium (triangle symbol, minor loop), and strontium (rectangle symbol) hexaferrites produced by CCSO. The inset shows the enlarged scale.

direction of easy magnetization in hexaferrite particles. As for the remnant magnetization M_r, the observed value was 35 and 25 emu/g, respectively, for $SrFe_{12}O_{19}$ and $BaFe_{12}O_{19}$. Intriguingly that for strontium and barium ferrite the calculated squareness ratio (SQR) $= M_r/M_s$ is about 0.6 and 0.7, respectively. In general, large SQR value is an important assessment of the quality of magnetic materials and critical in many applications such as magnetic recording media. The calculated SQR indicates that as-prepared ferrites apparently consist the randomly packed mono-domain granules. This assumption can be verified by calculating the critical size of singe domain particles using the formula:[20] $D_m = 9\sigma_w/2\pi Ms^2$, where $\sigma_w = (2k_BT_CK/a)^{1/2}$ is the wall density energy, K is the magnetocrystalline anisotropy constant, T_C is the Curie temperature, Ms is the saturation magnetization, k_B is the Boltzmann constant, and a is the lattice constant. In general, for $D < D_m$, the granules are mono-domain structures, while for $D > D_m$ the particles are multi-domain structures. The calculated value of D_m for $SrFe_{12}O_{19}$ and $BaFe_{12}O_{19}$ is about 620 nm and 1 μm, respectively. Since the observed particles size of strontium and barium ferrites, was shown above, is $\sim$60 nm it is able to conclude that the mono-domain structure of studied particles. On the other hand, the granules are not small enough to show the superparamagnetic behavior. In Figure 3 also shown the magnetization of strontium ferrite particles dispersed into PMMA, the moment normalized by mass of $SrFe_{12}O_{19}$ powder. The observed key parameters such as Hc, Ms, and Mr, as were expected, are very close to values for $SrFe_{12}O_{19}$ separated powder. Thus, the screen-printed strontium ferrite produced by CCSO method is a promising material for the magnetic applications.

CONCLUSIONS

The hard magnetic strontium- and barium-ferrite nanoparticles were produced by carbon combustion synthesis and were used to fabricate magnet structures by using screen-printing techniques. The purity of materials and nano-scale size of grains have been verified by XRD and SEM analyses. The synthesized hexaferrite $MeFe_{12}O_{19}$ (where Me-Ba or Sr) particles exhibit at room temperature the large values of anisotropy constant, saturation, and remnant magnetization, squareness ratio and enhanced coercivity, which can be explained by mono-domain morphology of particles. The use of nanoparticles instead of micron sized powders allows to better control scaling and dimensional accuracy of magnetic structures. The magnetic nanopowders consolidated by screen printing can serve as miniature permanent magnet structures for micro-sensors, -motors, -generators, -actuators, and micro electro-mechanical systems (MEMs) applications.

ACKNOWLEDGMENTS

We wish to acknowledge the financial support of this research by the National Science Foundation, Grant Nos. 0933140, 1126410, and 1138205.

[1]P. Campbell, *Permanent Magnet Materials and Their Application* (Cambridge University Press, Cambridge, 1994).
[2]H. Kojima, in *Fundamental Properties of Hexagonal Ferrites with Magnetoplumbite Structure: Ferromagnetic Materials*, edited by E. P. Wohlfarth (North-Holland, Amsterdam, 1982), Vol. 3, chap. 3.
[3]U. Topal, H. Ozkanb, and H. Sozeri, J. Magn. Magn. Mater. **284**, 416 (2004).
[4]S. Khizroev and D. Litvinov, J. Appl. Phys. **95**, 4521 (2004).
[5]Q. A. Pankhurst, J. Connolly, S. K. Jones, and J. Dobson, J. Phys. D: Appl. Phys. **36**, R167 (2003).
[6]M. Matsuoka, M. Naoe, and Y. Hoshi, J. Appl. Phys. **57**, 4040 (1985).
[7]G. Mendoza-Suarez, J. A. Matutes-Aquino, J. I. Escalante- Garcia, H. Mancha-Molinar, D. Rios-Jara, and K. K. Johal, J. Magn. Magn. Mater. **223**, 55 (2001).
[8]R. Varadinov, V. Nikolov, P. Peshev, I. Mitov, and Kh. Neykov, J. Cryst. Growth **110**, 763 (1991).
[9]M. V. Cabañas, J. M. González-Calbet, and M. Vallet-Regi, J. Mater. Res. **9**, 712 (1994).
[10]K. S. Martirosyan and D. Luss, AIChE J. **51**(10), 2801 (2005).
[11]K. S. Martirosyan and D. Luss, Ind. Eng. Chem. Res. **46**, 1492 (2007).
[12]K. S. Martirosyan, L. Chang, J. Rantschler, S. Khizroev, D. Luss, and D. Litvinov, IEEE Trans. Magn. **43**(6), 3118 (2007).
[13]K. S. Martirosyan, E. Galstyan, S. M. Hossain, Y.-J. Wang, and D. Litvinov, Mater. Sci. Eng., B **176**, 8 (2011).
[14]E. C. Stoner and E. P. Wohlfarth, IEEE Trans. Magn. **27**, 3475 (1991)
[15]B. T. Shirk and W. R. Buessem, J. Appl. Phys. **40**, 1294 (1969).
[16]S. Castro, M. Gayoso, J. Rivas, J. M. Greneche, J. Mira, and C. Rodríguez, J. Magn. Magn. Mater. **152**(1), 61 (1996).
[17]S. H. Gee, Y. K. Hong, F. J. Jeffers, M. H. Park, J. C. Sur, C. Weatherspoon, and I. T. Nam, IEEE Trans. Magn. **41**(11), 4353 (2005).
[18]Z. F. Zi, Y. P. Sun, X. B. Zhu, Z. R. Yang, J. M. Dai, and W. H. Song, J. Magn. Magn. Mater. **320**, 2746 (2008).
[19]A. Ataie and S. Heshmati-Manesh, J. Eur. Ceram. Soc. **21**, 1951 (2001).
[20]J. Smit and H. P. J. Wijn, *Les Ferrites* (Dunod, Paris, 1961).